

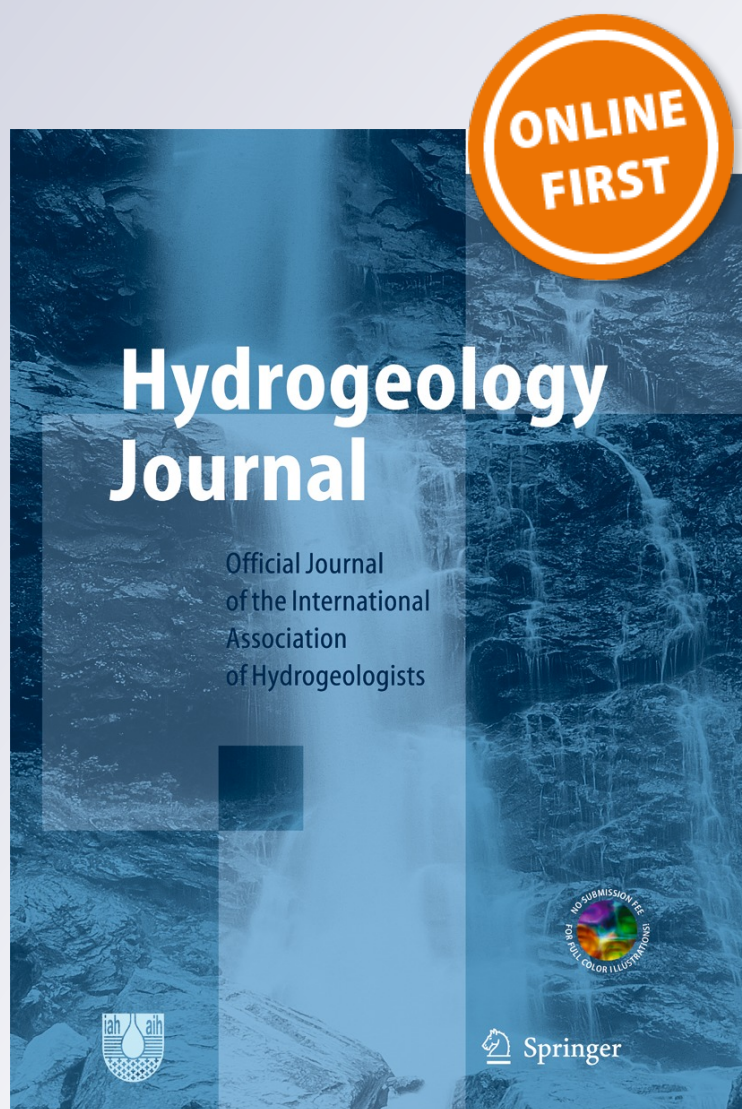
Olive-oil mill wastewater transport under unsaturated and saturated laboratory conditions using the geoelectrical resistivity tomography method and the FEFLOW model

P. Seferou, P. Soupios, N. N. Kourgialas, Z. Dokou, G. P. Karatzas, E. Candasayar, N. Papadopoulos, V. Dimitriou, A. Sarris, et al.

Hydrogeology Journal
Official Journal of the International
Association of Hydrogeologists

ISSN 1431-2174

Hydrogeol J
DOI 10.1007/s10040-013-0996-x



Your article is protected by copyright and all rights are held exclusively by Springer-Verlag Berlin Heidelberg. This e-offprint is for personal use only and shall not be self-archived in electronic repositories. If you wish to self-archive your article, please use the accepted manuscript version for posting on your own website. You may further deposit the accepted manuscript version in any repository, provided it is only made publicly available 12 months after official publication or later and provided acknowledgement is given to the original source of publication and a link is inserted to the published article on Springer's website. The link must be accompanied by the following text: "The final publication is available at link.springer.com".

Olive-oil mill wastewater transport under unsaturated and saturated laboratory conditions using the geoelectrical resistivity tomography method and the FEFLOW model

P. Seferou · P. Soupios · N. N. Kourgialas · Z. Dokou · G. P. Karatzas · E. Candasayar · N. Papadopoulos · V. Dimitriou · A. Sarris · M. Sauter

Abstract An integrated approach for monitoring the vertical transport of a solute into the subsurface by using a geophysical method and a simulation model is proposed and evaluated. A medium-scale (1m³) laboratory tank experiment was constructed to represent a real subsurface system, where an olive-oil mill wastewater (OOMW) spill might occur. High-resolution cross-hole electrical resistivity tomography (ERT) was performed to monitor the OOMW transport. Time-lapse ERT images defined the spatial geometry of the interface between the contaminated and uncontaminated soil into the unsaturated and saturated zones. Knowing the subsurface characteristics, the finite element flow and transport model FEFLOW was used for simulating the contaminant movement, utilizing

the ERT results as a surrogate for concentration measurements for the calibration process. A statistical analysis of the ERT measurements and the corresponding transport model results for various time steps showed a good agreement between them. In addition, a sensitivity analysis of the most important parameters of the simulation model (unsaturated flow, saturated flow and transport) was performed. This laboratory-scale study emphasizes that the combined use of geophysical and transport-modeling approaches can be useful for small-scale field applications where contaminant concentration measurements are scarce, provided that its transferability from laboratory to field conditions is investigated thoroughly.

Keywords Hydrogeophysics · Laboratory experiment · Transport modeling · Phenol

Received: 3 May 2012 / Accepted: 7 May 2013

© Springer-Verlag Berlin Heidelberg 2013

P. Seferou · M. Sauter
Department of Applied Geology, Hydrogeology and Environment
Geoscience (HEG), Georg-August Universität,
Göttingen, Germany

P. Seferou · P. Soupios (✉) · V. Dimitriou
Department of Natural Resources and Environment,
Technological Educational Institute of Crete,
P.O. Box 89, KDS Chania, 10, Anapavseos St,
73135 Chania, Crete, Greece
e-mail: soupios@chania.teicrete.gr
Tel.: +30-28-21023037
Fax: +30-28-21023003

N. N. Kourgialas · Z. Dokou · G. P. Karatzas
Department of Environmental Engineering,
Technical University of Crete,
Polytechniopolis, 73100 Chania, Greece

E. Candasayar
Department of Geophysical Engineering, Ankara University,
Tandogan Kampus, 06100 Ankara, Turkey

N. Papadopoulos · A. Sarris
Laboratory of Geophysical-Satellite Remote Sensing
& Archaeo-environment, Institute for Mediterranean Studies,
Foundation for Research and Technology, Hellas (FORTH),
Rethymnon, Crete, Greece

Introduction

A wide range of modern human activities (e.g. industrial processes, landfill, fertilizer and pesticide application, etc.) cause the release of different types of contaminants at the ground surface. These pollute the subsurface in many areas worldwide through spills, leaks, and, uncontrolled releases and disposals (Pankow et al. 1996; Rivett and Clark 2007; Tait et al. 2004).

The transport of contaminants with infiltrating water can cause serious problems with respect to groundwater quality. Remediation techniques alone are often not enough to completely recover the contaminated area. Thus, the use of real time monitoring or simulation methods to predict the solute transport mechanisms through the unsaturated zone has been a priority for geoscientists during the last few decades (Cassiani and Binley 2005; Bloem et al. 2010; Gasperikova et al. 2012; Müller et al. 2010). Laboratory experiments have been conducted to focus on contaminant transport processes in homogeneous or heterogeneous materials under confined or unconfined conditions. Through this experimentation, geophysical methods allow the estimation of subsurface properties (such as density, resistivity, velocity, magnetic

susceptibility, etc.) and can be a useful tool for hydrogeological investigations because they provide an additional data source for calibration of transport models, specifically in cases where scarce or no point data are available (Rubin and Hubbard 2005; Perri et al. 2012; Swanson et al. 2012; Ward et al. 2010). Although there have been many studies on the characterization of aquifer parameters using geophysical methods, very few have focused on the integration of geophysical imaging data with actual flow and transport models (Binley et al. 2002b; Coscia et al. 2012; Irving and Singha 2010; Jardani et al. 2012; Koukadaki et al. 2007). Binley et al. (2002a) used cross-borehole radar and cross-borehole two-dimensional (2D) and three-dimensional (3D) electrical resistivity tomography in order to monitor the migration of injected tracers in the unsaturated zone of a field site on the Sherwood Sandstone, in the UK. They used the pressure head, as derived from the one-dimensional (1D) moisture content distribution estimated from a borehole resistivity profile, to calibrate the 3D finite element model FEMWATER (Lin et al. 1997) for saturated media. Koukadaki et al. (2007) employed electrical resistivity tomography to obtain estimates of hydraulic conductivity while accounting for the karstic nature of the geological formations in a study area located east of the city of Heraklio in Crete, Greece. These estimates were employed as input in a groundwater flow numerical model (Princeton Transport Code, PTC) to estimate the hydraulic heads of the area of interest.

The electrical resistivity method is the most frequently used geophysical technique in hydrology as the subsurface resistivity strongly depends on the effective porosity, the degree of saturation and the pore-water conductivity. The method involves driving a known electric current between two electrodes and measuring the resulting potential differences between other pairs of electrodes. A transfer resistance to electric current flow is calculated which is defined as the ratio of the measured voltage to applied current. The changes in resistance observed from electrode grids at the surface or into boreholes (crosshole survey) are interpreted in terms of the direction and velocity of tracer migration in the saturated zone (Osienky and Donaldson 1995).

Electrical resistivity tomography (ERT) is a geophysical imaging technique that is used to estimate and present 2D and 3D models of the resistivity distribution of the earth interior. Data acquisition, processing and interpretation methodologies are widely described in the literature (e.g. Bentley and Gharibi 2004; Cassiani et al. 2006; Coscia et al. 2012; Doetsch et al. 2012; Johnson et al. 2012; Majken et al. 2008; Slater et al. 2002). The collected resistivity data are inverted to produce images of the subsurface; this is typically achieved by using regularized nonlinear least-squares algorithms (e.g. Candansayar 2008; Loke and Barker 1996) in which the forward problem is solved using either finite element or finite difference methods. ERT electrodes can be deployed either as surface or borehole arrays, or as a combination of the two. Moreover, the time-lapse mode (four-dimensional, 4D)

ERT provides spatial or volumetric subsurface information on resistivity changes in time, which are usually related to changes in saturation (both water and/or contaminant), temperature, and the composition of the pore fluid assuming a fixed geology (Karaoulis et al. 2011; Kim et al. 2009).

Cross-borehole electrical imaging involves the use of electrodes placed within two or more boreholes and the collection of numerous resistance measurements which are used to reconstruct the subsurface resistivity of the medium between the boreholes. Detailed information about the main concept of crosshole geoelectrical tomography is provided by Daily et al. (1992), Kemna et al. (2002) and Slater et al. (1997). In these studies, the reconstruction of temporally changing resistivity images caused by tracer migration was shown to provide useful hydrological information. The concept of field or laboratory-scale crosshole-electrical imaging as a method of investigating transport mechanisms in heterogeneous media is quite simple since the final model is constructed as the difference between an image during tracer injection and an image prior to tracer injection. Repeated imaging over time allows the identification of temporal changes in transport processes.

In recent years, many researchers have focused on performing laboratory-scale contaminant-transport experiments in soil columns under unsaturated or saturated conditions and comparing these results with computer simulation models. Various contaminants have been investigated by these studies such as nitrate (Al-Darby and Abdel-Nasser 2006), pesticides (Mirbagheri 2004; Mirbagheri and Monfared 2009), organic contaminants (Culver et al. 1997), volatile organic compounds (Rong 1999), etc.

Regarding olive-oil mill wastewater (OOMW), many researchers have investigated its treatment methods (Mantzavinos and Kalogerakis 2005; Tsagaraki et al. 2007) and its impact on soils (Moraetis et al. 2011; Zenjari and Neimeddine 2001; Piotrowska et al. 2006). However, to the authors' knowledge, no study has been conducted focusing on modeling the transport of OOMW through the subsurface, either in the field or on a laboratory scale.

This work focuses on investigating the vertical transport of OOMW in an unsaturated-saturated soil laboratory column using geophysical imaging data as a surrogate for contaminant concentration measurements in order to track the plume's movement. In order to increase the resolution of the resulted resistivity images, crosshole imaging was selected for this study to ensure that ERT image resolution was maintained with depth. The superior depth resolution that can be achieved using crosshole imaging relative to surface imaging is particularly important when characterizing and monitoring complex ground conditions and processes, where information is required at the scale of the heterogeneities. For simulating the solute transport, the finite element flow and transport model FEFLOW (Diersch 2009) was employed simulating the vertical transport of the studied contaminant under unsaturated and saturated conditions.

Experimental work-methods used

Preparation of the controlled experiment

An experimental tank with dimensions 1 m × 1 m × 1 m was constructed in order to perform the small-medium controlled laboratory experiment. A high performance material made of plexiglass with appropriate properties such as high transparency and durability, was used to construct the sides of the tank. This material facilitated the monitoring of the contaminant movement and the corresponding water-level changes. Initial stress analysis (static loads) using finite element software (ANSYS 2011) was implemented to guarantee the safe construction of the tank. Nine fluid valves were installed on the bottom of the tank as discharge points (Fig. 1a).

Four boreholes were constructed within the tank using plastic pipes (diameter about 3.5 cm) and twelve steel electrodes were installed at various depths in each borehole. The electrode spacing was appropriate for the given separation of the boreholes and the level of background noise (Bing and Greenhalgh 2000). Thus, an electrode spacing of 5 cm was used to obtain high-resolution data and improve the signal/noise (S/N) ratio. Moreover, the noise

reduction (low voltage) was accomplished by using high conductivity copper wires. The distance between the boreholes was 30 cm and the boreholes were located 35 cm away from the sides of the tank to minimize the boundary effects as much as possible.

Olive-oil mill wastewater (OOMW) as a contaminant

Olive oil production generates a large amount of solid and liquid wastes. This is a serious problem, causing contamination of groundwater in most of the Mediterranean countries (especially Turkey, Greece, Italy, Spain, and Portugal). The OOMW are water soluble and contain high concentrations of phenolic compounds, up to 80 g/L (APHA 1999). Usually, the OOMW are transferred to specially designed open tanks or spread directly on the soil, or even disposed of in adjacent torrents, rivers and lakes, posing a high risk to the environment. At the end of the olive harvesting season, the solid material from these tanks is collected and is either processed or properly deposited. The impermeability of these tanks/landfills is of crucial importance for preventing leaking of the wastes to the soil and possibly to the water resources. Escape of the



Fig. 1 a Sketch of the tank before construction and the valves designed at the bottom of the tank for different uses. b Piezometers used for controlling the water table. c Preparation of the container with OOMW before the initialization of the experiment. d Two different flow rates were used in order to simulate the annual deposition of the contaminant. The different flow rate values were used for the FEFLOW simulation

wastes to the environment can also occur by overflow of the liquid due to excessive deposition and/or rainfall (Lydakis-Simantiris et al. 2005). The release of phenol and its derivatives into the environment is of great concern. Phenolic compounds belong to a class of polluting chemicals, easily absorbed by animals and humans, and their toxicity is directed towards a great variety of organs and tissues (Smith et al. 2002).

The preceding reasons justify the use of OOMW as a contaminant for this experiment. The appropriate quantity of contaminant (OOMW) sample was taken from the Keritis River basin, an area near Chania on the island of Crete, Greece. It is known that environmental problems in this area are enormous (Lydakis-Simantiris et al. 2005). The physico-chemical parameters of the OOMW were chemically analyzed (Table 1); the phenol concentration is essential for the calibration of the FEFLOW simulation code. The OOMW is expected to be detectable by using the ERT method since the electrical conductivity (EC) of the contaminant wastewater and the EC of the drinkable water used for saturation of the soil material are 7.6 mS/cm (equal to 1.31 Ohm-m; Table 1) and 300 μ S/cm (33 Ohm-m), respectively (Seferou 2011).

Soil material

Since the time needed to get a unique 3D resistivity dataset is about 1 h and 30 min, it was decided to use fine-grained material, which would delay the percolation of the OOMW through the subsurface, thus making it possible to get time lapsed 3D ERT measurements. The hydraulic characteristics of the soil material used will be applied as initial data to the flow and transport model (FEFLOW). For that reason, hydraulic conductivity, void ratio and porosity were calculated as $k=1.09 \times 10^{-6}$ m/s, $e=0.312$ and $\varepsilon=23.77$ % respectively. The hydraulic conductivity and the porosity were determined by the falling-head laboratory method and the water evaporation method, respectively.

Acquisition configuration for 3D crosshole resistivity tomography: time-lapse geophysical modeling

Forty eight (48) electrodes were used for the 3D/4D resistivity data collection. Specifically, 4 boreholes 30 cm apart in both X and Y directions were installed. Each borehole contained 12 steel pin-type electrodes installed at 5-cm intervals. The last (the deepest) electrodes were installed at the depth of 0.582 m (0.418 m from the bottom) as is

shown in Fig. 2. The numbering of the 48 electrodes followed the counter-clockwise direction (Fig. 2a) starting the counting from borehole B1. Before the actual initialization of the experiment, a set of 1,812 apparent resistivity measurements (3D data set) were collected for reconstructing an accurate reference resistivity model which would be ultimately used for time-lapsed inversion and FEFLOW simulation. It should be noted that this number of readings (1,812) takes more than 90 min using a multi-electrode data acquisition system. In addition, it has been observed that if the distance between the boreholes is half of the total depth of the boreholes, the central part of the model can be "safely" reconstructed (Leontarakis and Apostolopoulos 2012). In this experiment, the distance between the boreholes is 30 cm and the depth of each hole is 60 cm ensuring that the centre of the resistivity model is recovered satisfactorily.

The software package EarthImager3D (EarthImager3D 2008; version 1.5.3) of Advanced Geosciences Inc. (AGI) was used for the inversion and time-lapse inversion of the apparent resistivity data sets collected in this experiment. The main idea is that the acquisition geometry is installed at fixed (permanent) locations (into boreholes in this case study) during the monitoring period to facilitate image comparison (EarthImager3D 2008). A successful time-lapse experiment requires the knowledge of a reference resistivity, which is reconstructed through the collection of a base data set. After that, the monitor survey is repeated with the same acquisition parameters.

According to Bing and Greenhalgh (2000), the cross-hole bipole-bipole (AM-BN measurement, where A and B are the current electrodes and M and N are the potential electrodes) configuration has the following advantages: (1) no remote-electrode effects, (2) it completely satisfies reciprocity, (3) adjustable sensitivity with different electrode spacing and (4) easy acquisition of field data in built-up areas. The configuration was also used in this study. Based on the aforementioned advantages, the cross-hole bipole-bipole AM-BN configuration was finally adopted based on synthetic data simulation examples.

Bipole-bipole (AM-BN) crosshole ERT measurements, with $a=5, 10, 15$ cm (a : electrode spacing) were collected along all possible combinations between the boreholes (B1–A1, B1–B2, B1–A2, A1–A2, A1–B2, A2–B2; Fig. 2a). The individual crosshole data sets were combined to a unique data file consisted of 1,812 readings. The single channel resistivity meter (Syscal R1 Plus) needed 1 h and 30 min to complete the measuring procedure.

Preparation of the laboratory experiment

At the beginning of the experiment, the tank was filled with the grained material (section [Soil material](#)) and water from the central valve at the bottom of the tank was injected in order to simulate an aquifer in a dry period (spring–summer). During the raising of the water level (from the bottom to the model surface) through the central valve, local soil subsidence among the boreholes was observed and some compacted cores (lenses) were

Table 1 Physico-chemical analysis of OOMW sample

Parameter	Value
pH	4.77
DO (dissolved oxygen), mg/L	0.22
EC (electrical conductivity), mS/cm	7.6
Phenols, mg/L	80
COD (chemical oxygen demand), g/L	22.3
Viscosity, mPa.s at 40 °C	93
Density, kg/m ³ at 20 °C	1,004.3

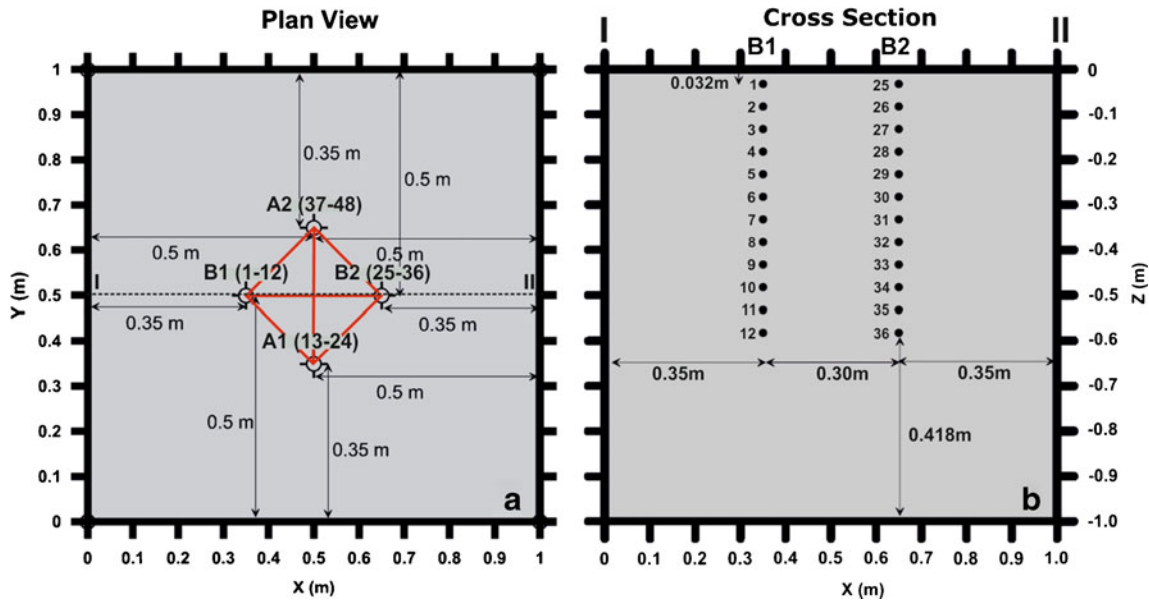


Fig. 2 a Plan view of the experimental configuration. The distances of boreholes from the sides of the tank are presented. The cross-borehole measurement was made between each borehole pairs (red lines) and all these data sets combined and used in the 3D inversion. b The cross section of the experimental geometry. The electrodes were installed every 5 cm (12 electrodes per borehole). For the 3D inversion, the 48 electrodes were assigned the numbering as presented in this figure—e.g. B1 (1–12), A1 (13–24), B2 (25–36) and A2 (37–48)

physically expected to be created and were indeed found (if possible due to the resolution of the geophysical measurements) through the ERT measurements. The ‘Brazil nut effect’ (Grossman 1997; Knight et al. 1993, 1996) could provide the necessary explanations regarding this physical phenomenon. Specifically, when water is injected suddenly (during the raising of the water table the particles were shaken or vibrated) into an inhomogeneous (consisted of various-sized grains) and incompressible (including the effects of air in spaces between particles) sedimentary column, the granular convection phenomenon can take place. The granular materials were subjected to shaking or vibration and exhibited a circulation pattern similar to fluid convection where the largest particles remained on top and the finer particles fell into the spaces underneath the larger particles after each shake. The aforementioned mechanism can create the compacted and/or impermeable lenses composed of the finer particles.

When the tank was fully saturated, all the valves (at the bottom of the tank) were opened and the tank was drained to a predefined level, creating unsaturated conditions at the top layers and saturated conditions at the bottom half of the tank. In order to avoid measuring instabilities (since the experiment should be fully controlled and the water table should be predefined), the experiment (geo-electrical measurements) started a week (7 days) after the first dewatering of the tank. This time period allowed the water table to stabilize at the predefined level after the continuous infiltration of the water from the unsaturated zone.

The contaminant container, able to store 60 L of wastewater liquid, was also placed on the top of the experimental tank as is shown in Fig. 1b,c). The purpose was to release the contaminant at the center of the tank and between the boreholes (Fig. 1d).

After the water level was stabilized within the tank, a reference ERT data set was collected. The first data set was sampled twice using two resistivity instruments to ensure the repeatability and accuracy of the measurements. All the data files were collected by using the IRIS Syscal R1 Plus Switch 48 and the crosschecking was accomplished with the IRIS Syscal Pro.

The injection of the OOMW was performed with two different flow rates representative for the annual deposition of the contaminant. The first data set was collected as a reference data file. After 15 min, the acquisition of the 2nd data file was started, and the OOMW was released with a controlled flow rate of about 250–270 ml/h. Two-dimensional crosshole ERT measurements (by using 24 electrodes) were continuously captured every 15 min. In total, 77 crosshole resistivity data sets were acquired. After about a day (25 h and 13 min), the flow rate was changed to 697 ml/h and eight supplementary resistivity (3D) data files were collected approximately every 12 h, using four borehole electrodes (in total 48 electrodes). Four piezometers (Fig. 1b) that were installed in the tank were used to control and keep the water-level stable (to the predefined level) since the water-level changed (raised) due to the contaminant release.

130 h after the initialization of the experiment, the last 3D data set was collected and the acquisition procedure was terminated. The data-quality control was checked by applying noise reduction, filtering and bad datum removal before the 2D, 3D and time lapse (4D) inversion.

3D inversion

The minimum voltage should be set close to the hardware resolution or the environmental noise level. Any signal

less than 1 mV is usually too small to measure accurately. Thus, the data that measured voltage less than 1 mV were removed before the inversion. The effect of the tank's boundary was incorporated into the inversion. The model mesh consists of 2,662 cubes (in X, Y, Z directions 11, 11 and 22 cubes, respectively were used).

For the inversion, the smoothness-constrained least-squares approach is used (Candansayar 2008; Sasaki 1992). In this approach the following rectangular system is solved in each iteration (Candansayar 2008; Sasaki 1994);

$$\begin{bmatrix} \mathbf{W}_d \mathbf{A} \\ \sqrt{\alpha} C \end{bmatrix} \Delta \mathbf{m} = \begin{bmatrix} \mathbf{W}_d \Delta d \\ 0 \end{bmatrix} \quad (1)$$

where \mathbf{A} is the sensitivity (Jacobian) matrix, $\Delta \mathbf{d}$ is the vector of differences between the measured and the calculated data, $\Delta \mathbf{m}$ is the parameter correction vector, C is the Laplacian operator, \mathbf{W}_d is the data weighting matrix and α is a regularization parameter. There are various suggestions for selecting α . In this work, a cooling approximation (Candansayar 2008; LaBrecque et al. 1997) is used. An initial value of 10 is selected (as suggested by EarthImager3D developer) and it is decreased at each iteration. A homogenous half-space is used as an initial model and the average of measured apparent resistivities for all electrode separations is used as the resistivity initial model.

The maximum number of iterations and the misfit between the measured and calculated data for a reconstructed model (root mean squares, RMS) were used as convergence criteria for acquiring the final resistivity model. The average number of iterations and RMS to achieve the final inverted models were about 8 and 2.3 %, respectively.

4D time-lapse inversion

The optional "4D time-lapse inversion" module (EarthImager3D 2008) is used for monitoring the contaminant diffusion to the subsurface. At first, a reference resistivity data set was collected in order to establish a base resistivity model of the site. Afterwards the monitor survey was repeated during the period of monitoring with the same command file as the one used in the base survey. In total, 84 data sets were collected in a time period of 130 h. The time-lapse inversion algorithm takes advantage of the base survey data and base resistivity model. Instead of inverting the monitor data set alone, the EarthImager3D algorithm inverts the difference (difference inversion) between the monitor and base data sets. Difference inversion combines the inversion of the reference (base) dataset and time-lapse inversion of a single monitor dataset in one step. Moreover, the base resistivity model is used as the a priori model in the time-lapse inversion. Therefore, the time-lapse inversion converges faster than standard inversion and is more sensitive to small subsurface changes. The inherent inversion artifacts may be cancelled in the difference images (EarthImager3D 2008).

At the end of difference inversion, percent differences of resistivity images were created. It is usually preferred to set the absolute value of minimum and maximum plot bounds to be equal, so zero (no change) will be in the center of the color scale and in a green color by default.

FEFLOW simulation

For the purpose of modeling the OOMW transport through the laboratory column, the finite element subsurface flow and transport simulation code named FEFLOW (Diersch 2009) was used. The FEFLOW software has been successfully applied in laboratory and field-scale applications. Some recent papers include Dokou and Karatzas (2012), Jakovovic et al. (2011), and Peleg and Gvirtzman (2010). The basic equations used by FEFLOW under unsaturated-saturated conditions for flow and mass transport are derived from the macroscopic-phase-related conservation principals of flow, mass, momentum and energy resulting in the following non-linear system of equations (Diersch 2002):

$$[S_o \cdot s^f(\psi) + \varepsilon \cdot C(\psi)] \frac{\partial h}{\partial t} + \nabla \cdot \mathbf{q} = Q_h \quad (2)$$

$$s^f(\psi) \varepsilon R_d(C) \frac{\partial C}{\partial t} + \mathbf{q} \cdot \nabla C - \nabla \cdot [(\varepsilon s^f(\psi) D_d \mathbf{I} + \mathbf{D}) \times \nabla C] + [s^f(\psi) \varepsilon R(C) \partial + Q_h] C = s^f(\psi) Q_c \quad (3)$$

The preceding equations are coupled with Darcy's law, described by the following:

$$\mathbf{q} = -K_r(s^f) \mathbf{K} \nabla h \quad (4)$$

where:

- S_o specific storage coefficient (compressibility)
- ψ pressure head
- s^f water saturation
- ε porosity
- C contaminant concentration
- h hydraulic head
- \mathbf{q} Darcy's velocity
- Q_h lumped balance flux of fluid
- R_d derivative term of retardation
- D_d molecular diffusion
- \mathbf{I} unit (identity) tensor
- \mathbf{D} tensor of hydrodynamic dispersion
- R retardation factor
- Q_c contaminant mass source/sink
- K_r relative conductivity
- \mathbf{K} hydraulic conductivity tensor

In order to solve the preceding system of equations, constitutive relationships for the following parameters have to be determined: moisture capacity, $C(\psi)$, and relative hydraulic conductivity, $K_r(s^f)$. For this purpose, the van Genuchten parametric model described by the equations below was applied (Diersch 2002):

$$s_e^f = \begin{cases} \frac{1}{[1 + (A|\psi|)^n]^m} & \text{for } \psi < 0 \\ 1 & \text{for } \psi \geq 0 \end{cases} \quad (5)$$

$$K_r = (s_e^f)^{\frac{1}{2}} \left\{ 1 - \left[(s_e^f)^{\frac{1}{m}} \right]^m \right\}^2 \quad (6)$$

$$s_e^f = \frac{s_r^f - s_r^f}{s_s^f - s_r^f} \quad (7)$$

where:

- s_e^f effective saturation of fluid
- A, n, m van Genuchten curve-fitting parameters
- s_r^f residual saturation
- s_s^f maximum saturation

Under saturated conditions ($s^f=1$), the non-linear equations reduce to a linear system (Diersch 2002). The Freundlich isotherm describing the absorption process was chosen:

$$R = 1 + \frac{(1-\varepsilon)}{\varepsilon} b_1 \times C^{b_3-1} \quad (8)$$

$$R_d = 1 + \frac{(1-\varepsilon)}{\varepsilon} b_1 \times b_2 \times C^{b_2-1}$$

where:

- b_1, b_2 = Freundlich sorption coefficient and exponent, respectively

The contaminant injection into the laboratory soil column was described by a “well” boundary condition in FEFLOW. The rate of diffusion decreases with decreasing moisture content. A linear relationship between the diffusion coefficient and the moisture content has been reported by Badv and Faridfarid (2005).

FEFLOW model and parameters

A conceptual model of the laboratory column was created based on the extent of the unsaturated and saturated zones as well as the heterogeneity of the packed medium and is

shown in Fig. 3. The unsaturated zone (extending 0.25 m from the column surface) was partitioned into 5 layers (layers 1–5) and the saturated zone into 9 layers (layers 6–14). The vertical discretization of the unsaturated zone is denser because of the nonlinearity of the governing equations in this zone. The thickness of layers 5 and 8, which contained strongly compacted lenses, was estimated by observation from the geophysical images/modeling. The geophysical column extends from layer 1 to layer 10. The horizontal discretization of the model domain was implemented using a triangular finite element mesh consisting of 16,900 nodes and 29,736 elements. The hydraulic head is held constant throughout the model. The initial hydraulic head distribution for all layers was set to 0.75 m and a constant head of 0.75 m was applied to the layers of the saturated zone (Layers 6–14).

Regarding the hydraulic conductivity parameter, an estimate was available from laboratory measurements for the saturated zone equal to 1.09×10^{-6} m/sec. For the unsaturated zone the hydraulic conductivity value for each layer was calculated by the model using Eq. (6). The hydraulic conductivity of the low permeability lenses was set 3 orders of magnitude lower than the saturated hydraulic conductivity (Table 2). The hydraulic conductivity parameter was considered isotropic in all layers. For the solution of the problem under unsaturated conditions, the van Genuchten parametric model was applied using the following parameters that correspond to sand soil media: $n=3$, $A=1.2$, residual saturation $S_r=0.12$ and maximum saturation $S_s=1$ (van Genuchten 1978).

A time-dependent type of mass-transport boundary was applied in the first model layer to account for the fact that the contaminant flux was changed during the experiment. A well-

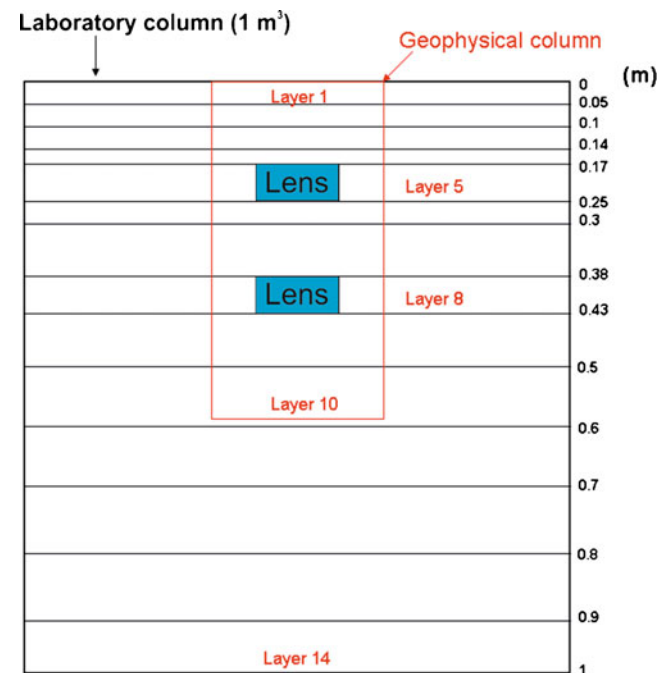


Fig. 3 Schematic representation of the conceptual model for FEFLOW modeling

Table 2 The main parameters that were used in the FEFLOW model - calibration values

Parameters	Unsaturated zone layers (1–5)	Saturated zone layers (6–14)
Hydraulic conductivity, (m/s)		
Sand	Calculated by the model	$K_{xx}=K_{yy}=K_{zz}=1.09 \times 10^{-6}$
Lens	Calculated by the model	$K_{xx}=K_{yy}=K_{zz}=1.09 \times 10^{-9}$
van Genuchten parameters		
S_r (residual saturation), (cm^3/cm^3)	0.12	-
S_s (maximum saturation), (cm^3/cm^3)	1.0	-
A (cm^{-1})	1.2	-
n	3	-
Mass transport boundaries (MTB)		
0–1 day, (mg/l , m^3/day) ^a	0.5	0.5
1.001–6 days, (mg/l , m^3/day)	1.33	1.33
Sorption parameters		
b_1 (sand)	0.3219	0.3219
b_1 (lens)	0.2123	0.2123
b_2 (sand)	1.3896	1.3896
b_2 (lens)	2.0581	2.0581
Molecular diffusion, (m^2/s)		
Layer 1	5.7×10^{-7}	-
Layer 2	5.9×10^{-7}	-
Layer 3	6.1×10^{-7}	-
Layer 4	6.5×10^{-7}	-
Layer 5	6.8×10^{-7}	-
Layers 6–14	-	2.3×10^{-6}

^a Two units were used for MTB. One unit is concentration and the other the volumetric rate, which gives the mass rate of OOMW.

type boundary condition that combines the initial concentration of the contaminant with its flux was also applied.

Olive-oil mill wastewaters contain many different contamination components. In this study, phenols were chosen as a typical contaminant because of their strong toxicity and high concentration in OOMW (Moraetis et al. 2011). The specific phenols contained in this sample, according to the chemical analysis of the OOMW sample, are appreciably soluble in water. Based on this evidence, a single-phase numerical model such as FEFLOW can be used to simulate the phenol contaminant transport. The selection of a single-phase model is also justified by the fact that the sample density measurement ($1,004.3 \text{ kg/m}^3$ at $20 \text{ }^\circ\text{C}$) is very close to that of water.

The initial phenol concentration was measured at 80 mg/l and the initial flux for the first day of the experiment was 260 ml/h or $0.00624 \text{ m}^3/\text{day}$. Thus, the well-type boundary condition value was: $80 \text{ mg/l} \times 0.00624 \text{ m}^3/\text{day} = 0.5 \text{ mg/l m}^3/\text{day}$. For the rest of the experiment the contaminant flux was held at 697 ml/h or $0.0167 \text{ m}^3/\text{day}$. Based on the aforementioned, the well-type boundary condition value was: $80 \text{ mg/l} \times 0.0167 \text{ m}^3/\text{day} = 1.33 \text{ mg/l m}^3/\text{day}$.

The values for the sorption parameters were based on the experimental work of Fiore and Zanetti (2009) who investigated the behavior of phenols for different soil types and phenolic solutions at different pH values. According to their work, for conditions similar to this study (phenolic solution at pH close to 4), the sorption isotherms can be accurately described by the Freundlich model for samples that contain mostly calcite sand (corresponding to the main porous medium in this experiment) and a mixture of clay, silt and calcite sand (corresponding to the low permeability lenses in this experiment). The sorption coefficients that were calculated

in each case are $b_1=0.3219$ and $b_2=1.3896$ for the sand sample and $b_1=0.2123$ and $b_2=2.0581$ for the low permeability sample (lenses). The measured porosity value was 0.24 and the storativity parameter was set at 0.2 for all model layers.

The main challenge of this modeling process was to link the model concentrations with the geophysical images. Because no phenol concentration measurements were available in this study (apart from the initial concentration) and in order for the ERT results to be used as calibration data for the groundwater transport model, a detection limit for the phenol concentration that corresponds to the edge of the ERT plume had to be specified. This limit was estimated during the calibration process that was performed using a trial and error technique. Various values for the phenol concentration limit were tested until the optimal value of 10 mg/l was established. This value procured the best match between the ERT data and the model concentration results for the vertical movement of the OOMW contaminant and is considered large enough to be detected by the geophysical sensors, taking into account that the initial phenol concentration in the OOMW product was 80 mg/l .

Due to the fact that the process of diffusion is the driving force of the movement of OOMW through the soil column, the model calibration process was performed simultaneously on the phenol detection limit and the diffusion parameter. For the diffusion parameter, a range of appropriate values for the saturated zone ($5 \times 10^{-9} - 5 \times 10^{-6} \text{ m}^2/\text{s}$) was obtained by Herbert et al. (1988). The final calibrated value was $2.3 \times 10^{-6} \text{ m}^2/\text{s}$ for the saturated zone. For the unsaturated zone, different diffusion parameter values were used for each layer as a result of the calibration process. As the moisture content increases from the top layer (layer 1) to layer 5, the diffusion

parameter increases as well. The calibrated values that were used for each layer are shown in Table 2.

Results

Crosshole resistivity tomography

The experiment started on 24 June 2011 taking several 2D/3D (reference) data sets before the OOMW release. The 3D crosshole resistivity tomography of the reference model shows an average resistivity value of about 60 Ohm-m. Additionally, two high resistivity areas with values ranging around 90–120 Ohm-m at the depths of 23 and 40 cm were depicted (Fig. 4). The very low resistivity (3–8 Ohm-m) areas can be assumed as inversion artifacts since they were found at the edges of the model.

The final resistivity tomographic models for seven different time steps are presented in Fig. 5a–g by using the isosurfaces presentation (resistivities between 1 and 20 Ohm-m are visible). The first 3D image (Fig. 5a) shows that 63 h after the “release of the contaminant onto the surface (RCS)”, the contaminant front reached the depth of 18 cm. The anomalies at the bottom of the model can be discarded assuming that they were artifacts (numerical instabilities) from the application of the inversion algorithm. Figure 5b shows that the contaminant reached the depth of 22.5 cm (73 h after RCS) and the high resistivity lens is also confirmed by the interpretation of the 3D resistivity data. Figure 5c shows that after 82 h the contaminant moved downward to the depth of 27 cm moving around the high resistive (impermeable) lens. Figure 5d,e shows the contaminant movement to the depth of 33 and 34 cm, respectively. It is worth mentioning that after the contaminant passes around the impermeable (high resistive) lens at the depth of about 23 cm, it is unified again at the depth of 36 cm (Fig. 5f). Finally, Fig. 5g

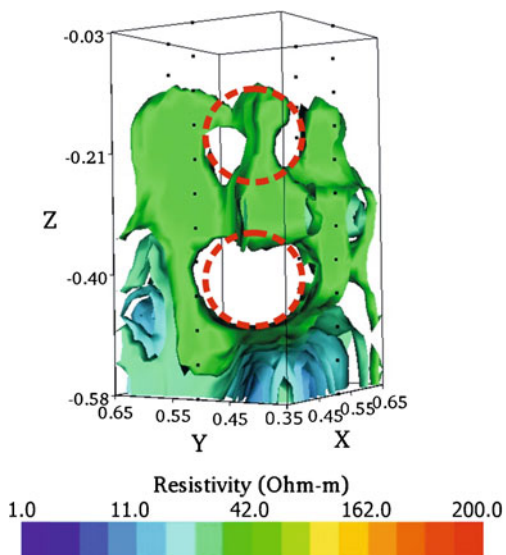


Fig. 4 3D crosshole resistivity tomography taken on 26 June before the beginning of the experiment. Only low resistivity isosurfaces are visible, indicating the possible presence of two high resistive (impermeable) bodies (*dashed red-line circles*) at the average depths of 23 and 40 cm (axes units are shown in meters)

shows that after 130 h the main body of the contaminant (wetting front) has reached the depth of 40 cm exhibiting a higher velocity at the center of the front, as expected.

4D time-lapsed inversion

Figure 6a–f presents the percent differences of resistivity images after the application of 4D time-lapsed inversion. The images show similar results with the 3D ERT tomographic images as presented in Fig. 5a–g regarding the movement of the OOMW front.

FEFLOW results and comparison with ERT images

For the comparison between the FEFLOW results and the geophysical images, six characteristic time steps were chosen: $t_1=8\text{ h}=0.34\text{ days}$, $t_2=15\text{ h}=0.625\text{ days}$, $t_3=82\text{ h}=3.4\text{ days}$, $t_4=94\text{ h}=3.9\text{ days}$, $t_5=106\text{ h}=4.4\text{ days}$, $t_6=130\text{ h}=5.4\text{ days}$ (Fig. 7). A visual comparison was performed between the geophysical images (2D cross-section or 3D) and the 2D concentration contour plot of the layer that the plume has reached at each time step. For each time step, the contaminant plume is considered to have reached a specific model layer if the simulated phenol concentration of this layer exceeds the limit of 10 mg/l (Fig. 8), which was previously specified (see section *FEFLOW model and parameters*) during the calibration process.

At time step $t_1=0.34\text{ days}$, the measured contaminant plume reached model layer 4, according to the geophysical image. This layer was reached by the simulated contaminant plume at a slightly earlier time (0.3 days), as depicted in Fig. 7 (layer 4), indicating a very good fit between observed and modeled results for this early time step.

At time step $t_2=0.625\text{ days}$, the geophysical image indicates that the measured contaminant plume reached model layer 5 (lens layer) and covered the entire layers 1–4, a fact that was confirmed by the simulation model although the concentration limit was reached at a slightly earlier time in this case as well (0.56 days), as shown in Fig. 7, layer 5.

For time step $t_3=3.4\text{ days}$, the plume reached layer 6 according to the corresponding geophysical image. In this case, the time indicated by the simulation model (3.46 days) was in very good agreement to the real time (Fig. 7, layer 6). Moreover, the 2D simulated concentration plume for layer 6 shows that the plume’s transport is hindered by the low permeability (high resistivity) lens located in the layer directly above it. The plume moves around the lens in order to reach the lower layers, as is also the case in the lab experiment, indicated by the corresponding 3D geophysical image.

For the next time steps ($t_4=3.9\text{ days}$, $t_5=4.4\text{ days}$, $t_6=5.4\text{ days}$) the corresponding layers that the measured plume has reached according to the geophysical images are layers 7, 8 and 9, respectively (Fig. 7). These layers are reached by the simulated plume in somewhat later times of 4.0, 5.2 and 5.9 days, respectively.

It is observed that in the unsaturated zone, the time it takes for the contaminant to reach the corresponding model layer is always slightly smaller than the time

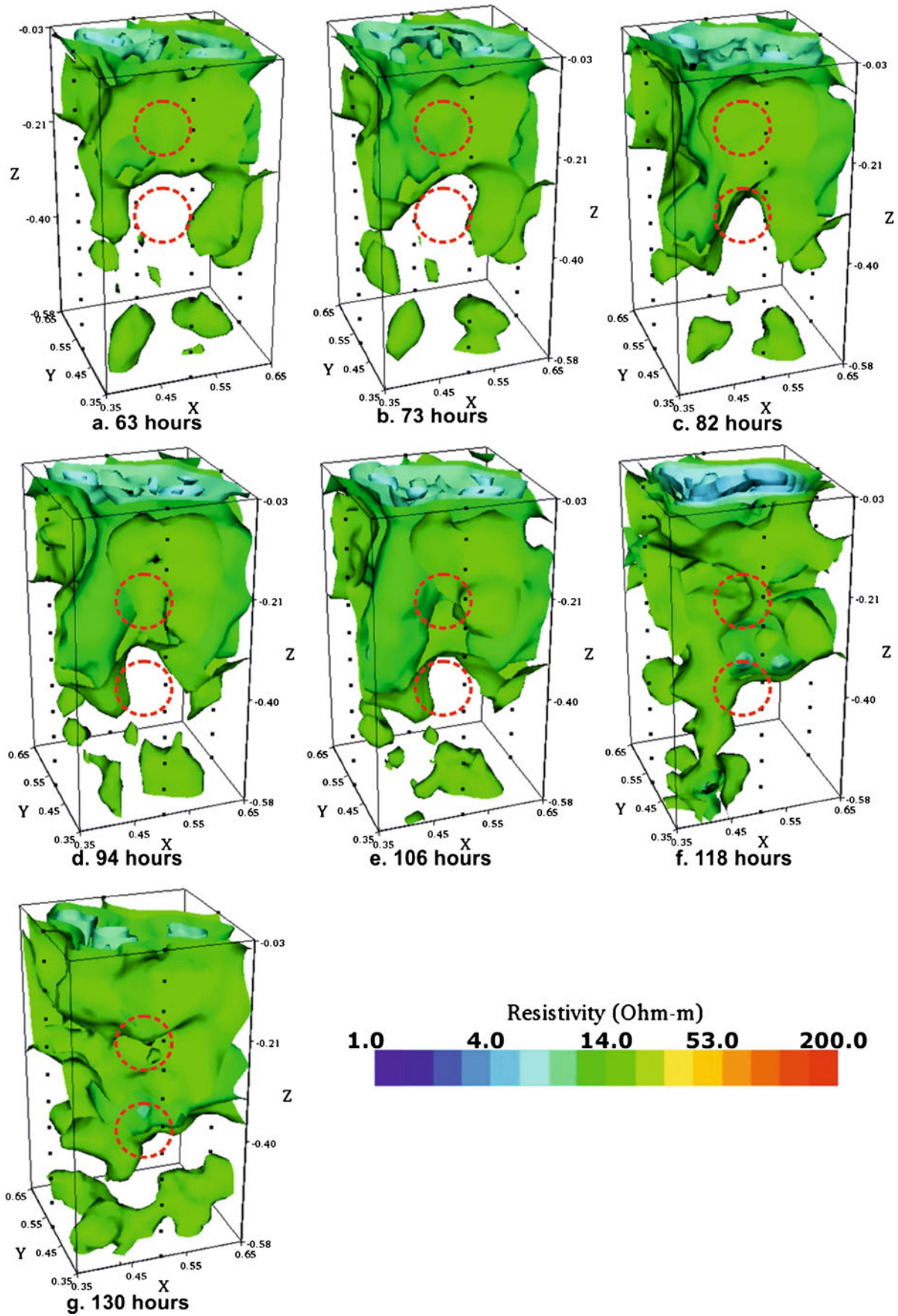


Fig. 5 a–g Final 3D resistivity models presented as isosurfaces. 1–20 Ohm-m resistivity surfaces are visible

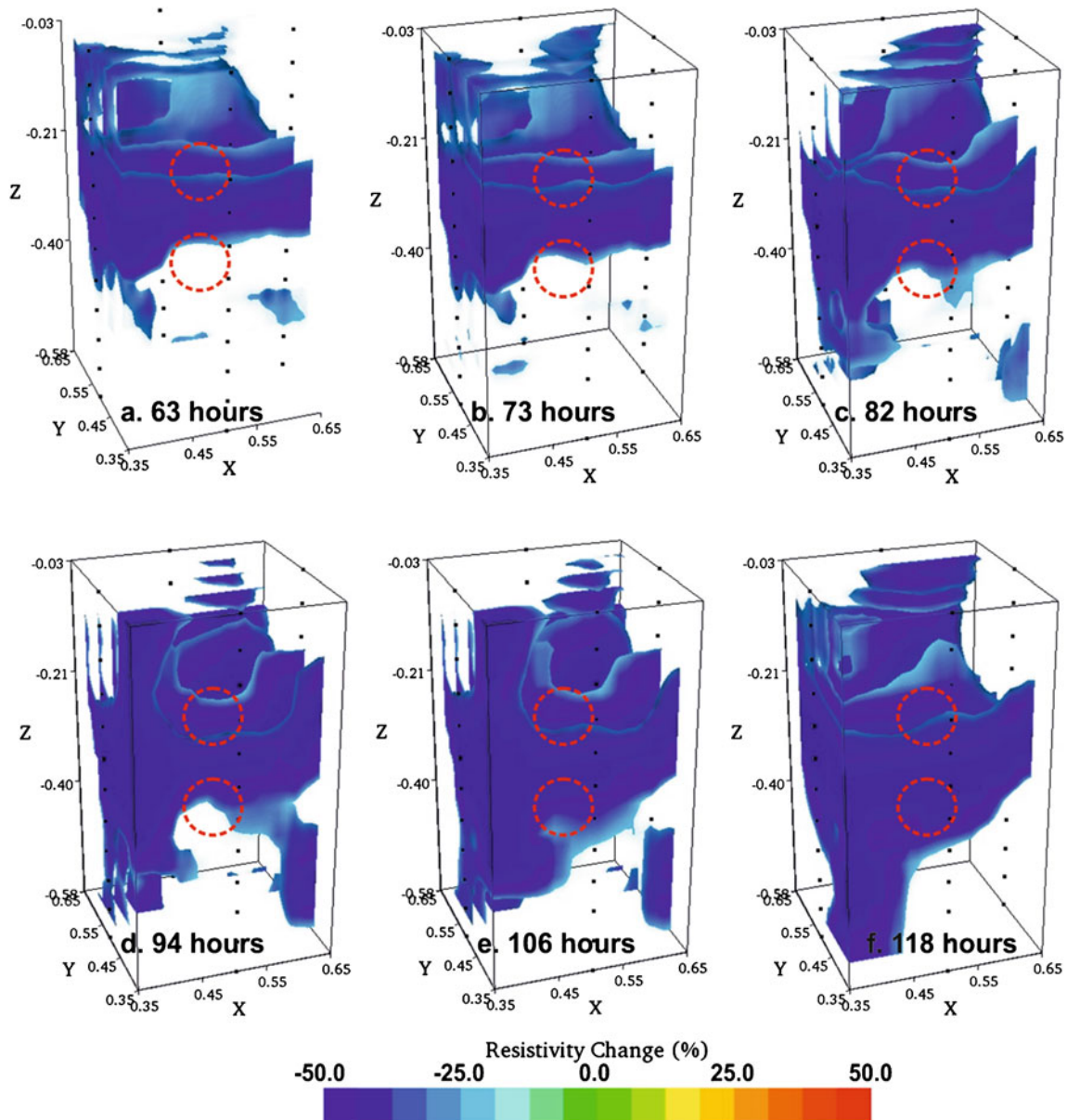


Fig. 6 4D time-lapsed difference inversion for 6 time steps—63 h (a), 73 h (b), 82 h (c), 94 h (d), 106h (e), and 118 h (f) after the beginning of the controlled experiment

indicated by the geophysical images while in the saturated zone the exact opposite behavior is observed.

Statistical analysis

In order to quantify the accuracy of the calibration process, a statistical analysis was performed between the ERT times and the corresponding transport model times. Specifically, two common statistical measures, R^2 and root mean square error (RMSE), were employed in this study. The results show a good fit between the time data, with an R^2 equal to 0.99 and a RMSE equal to 0.41 days. This analysis evaluates only the goodness of fit in the vertical direction and does not take into account the horizontal

extent of the plume, because such an evaluation was not possible and, since there was no head gradient in the soil column, the main focus of this study was the vertical transport of the OOWM. This leads to very good calibration results, which might be misleading because of various reasons that can reduce the actual model accuracy. The calculation of the statistical parameters is based on very few data points, the comparison is based on visual observation, the method exhibits a significant degree of uncertainty, and the calibration procedure includes the trial and error technique for the determination of the phenol concentration detection limit, which played a catalytic role in the improvement of the calibration result.

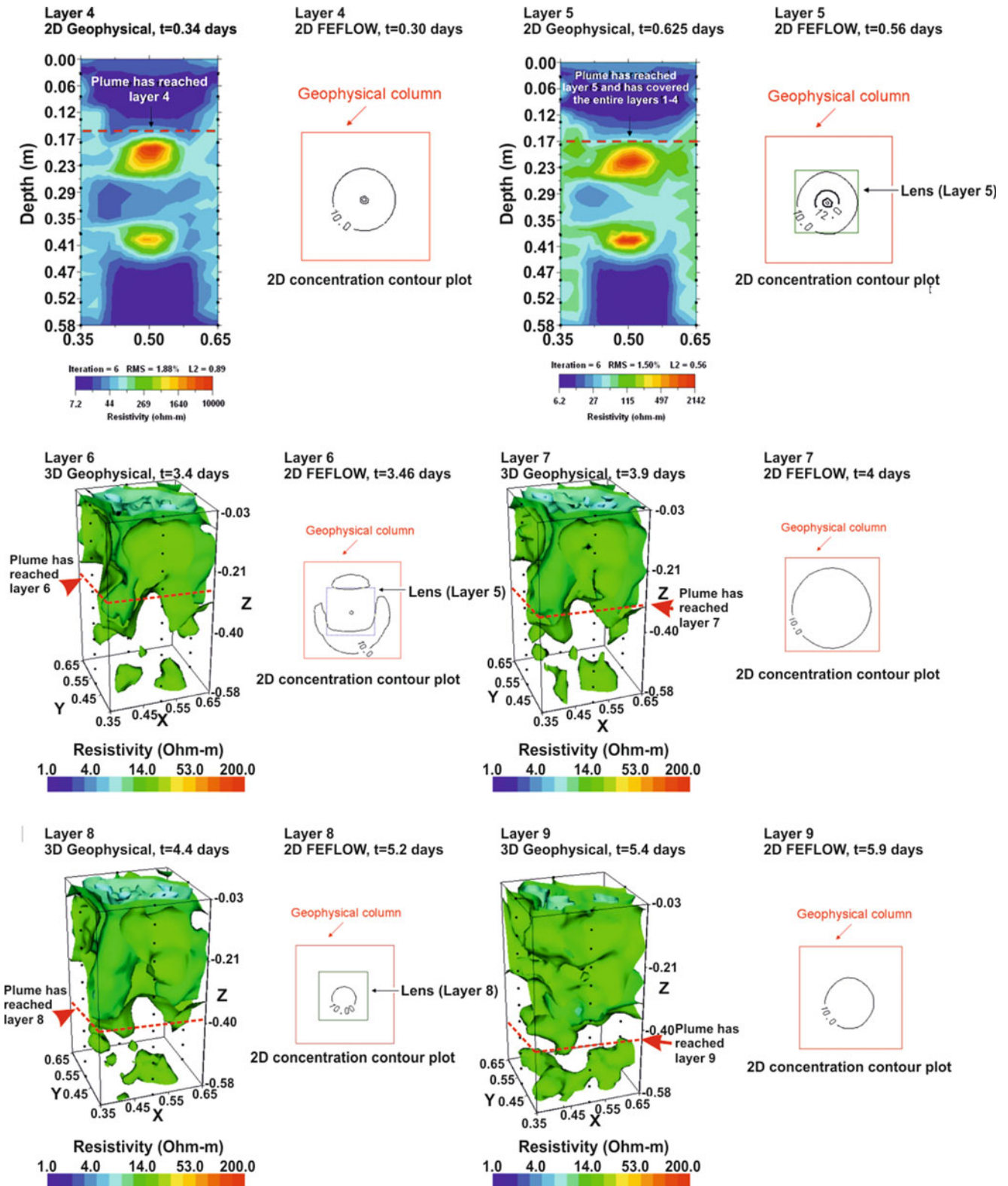


Fig. 7 Comparison between geophysical and FEFLOW model results for the unsaturated (layers 4 and 5) and saturated (layers 6, 7, 8 and 9) zones

Sensitivity analysis of the FEFLOW model

A sensitivity analysis of the hydraulic conductivity (K), porosity (ε) and van Genuchten parameters (A and n) was performed in this study, in order to assess how

these input parameters affect the model output. These specific parameters were chosen because they exhibit the most uncertainty among the input data and each represents a main component of the simulation model:

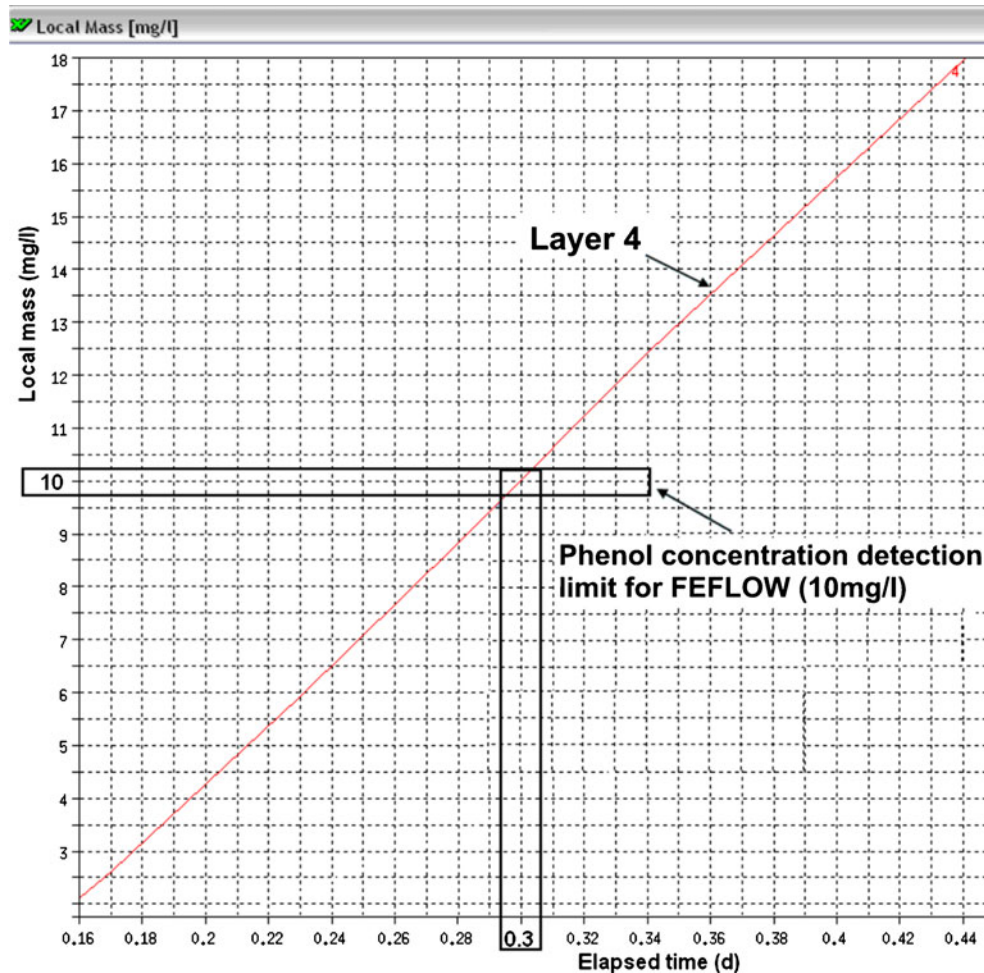


Fig. 8 Determination of the time when the simulated contaminant plume reaches layer 4 based on the 10 mg/l limit

(1) van Genuchten parameters (A) (unsaturated flow component), (2) hydraulic conductivity (flow component) and (3) porosity (transport component). Specifically, the objective is to study how the uncertainty in these four factors affects the time that the OOMW needs to reach each layer in the unsaturated and saturated zones.

For this propose, reasonable perturbation percentages (± 10 and ± 20 %) were applied to the calibrated parameter values and the change in the time needed for the OOMW to reach the corresponding layers was computed. Figure 9 presents the change of the estimated time (%), for each parameter and perturbation percentage. As can be concluded from this figure, for hydraulic conductivity all the perturbation percentages have small effect in the estimated time for each layer, apart from layer 5 (L5) in the unsaturated zone and layer 8 (L8) in the saturated zone, which show a significant impact. These layers are the ones where the low permeability lenses are located, a fact that shows the significance of heterogeneity of a porous medium on the transport process. Specifically, the effect is more prominent for the positive perturbation percentages,

indicating that when the lenses become more permeable, the effect on the time needed to reach the specific layer is intensified, an effect that is not as severe when the lenses become less permeable.

For the porosity, the applied perturbation percentages have the largest impact on the time change that reaches 20 % in the upper layers (L4 and L5). This effect is extenuated with depth, as can be seen in Fig. 9. In case of the other two factors, van Genuchten parameters (A and n), the time changes were relatively small and not greater than 0.6 % for all layers. Thus, in this study, it is evident that porosity is the most sensitive parameter for the FEFLOW modeling.

Discussion

Direct current resistivity (DCR) is a widely used method for the investigation of subsurface systems that generally gives satisfactory results. However, its applicability could be limited in large-scale field applications, especially if dealing with highly heterogenous systems where the geology and hydraulic conductivity distribution are not well known. If the proposed methodology is to be applied in the field, existing boring logs

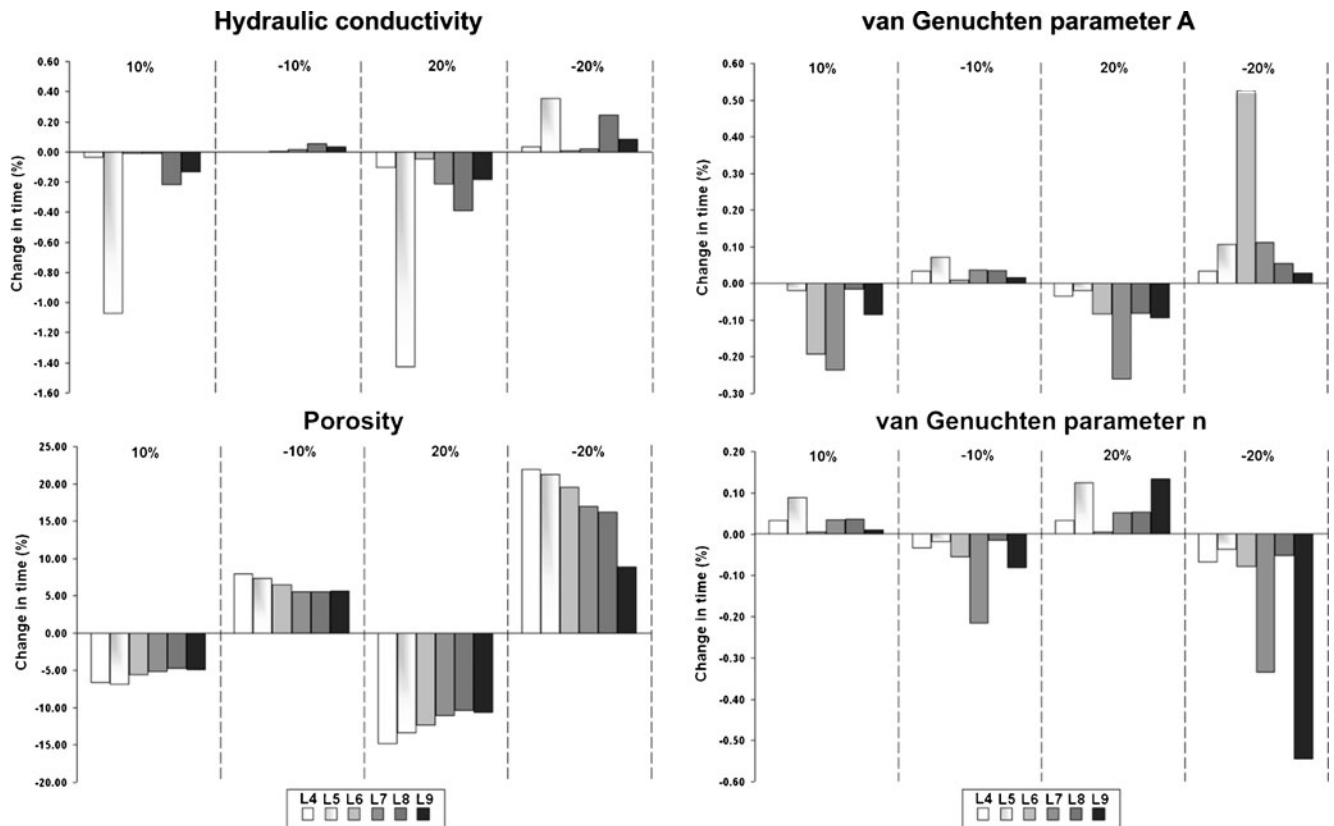


Fig. 9 Sensitivity analysis of the FEFLOW model

and pumping test results could be used in order to obtain useful information about the geology and hydraulic conductivity of the subsurface. This hydrogeological information could then be used as a priori information for the 3D DC resistivity data inversion in order to increase the accuracy of the resistivity model of the complex study area.

Moreover, DCR results in variable saturated media usually exhibit high uncertainty that is very difficult to control or quantify. This fact can be related to the non-uniqueness of the inversion of DCR data. However, in laboratory conditions, as is the case in this study, it is easier to control both the heterogeneity and the variable saturation conditions of the porous medium, reducing the uncertainty of the process.

The objective of this work was to provide an “environmental monitoring tool” by combining geophysical imaging data with transport modeling in order to monitor contaminant migration. ERT data can provide real-time monitoring and can be a useful tool for the calibration of transport models providing an additional data source, especially in cases where scarce or no point-contaminant-concentration data are available. This can only be accomplished though, if a link between the transport model concentrations and the geophysical images exists. In this work, since no actual phenol concentration measurements were available, this link was established by determining a detection limit for the phenol concentration (10 mg/l) that corresponds to the edge of the ERT plume using a trial and error technique.

The statistical analysis of the results shows a very good agreement between the ERT times and the corresponding transport model times. It should be noted though that this analysis evaluates only the goodness of fit in the vertical direction and does not take into account the horizontal extent of the OOWM plume. In addition, the calculation of the statistical parameters is based on very few data points and the comparison is based on visual observation. However, there is a small mismatch between the arrival times of the contaminant on the ERT data and the transport simulation. This mismatch could be attributed to the water drainage at the bottom of the tank that might have affected the contaminant migration and so the ERT images.

The present methodology seems to be effective in laboratory scale; nevertheless, its transferability in the field is a task that should be investigated thoroughly. Specifically, as mentioned in the preceding, in order to be able to obtain sufficient time-lapsed 3D ERT measurements, the hydraulic conductivity of the porous media should be relatively low to allow a small percolation rate. In addition, it was found through the sensitivity analysis of the transport model that the porosity is the most sensitive parameter; thus, in field applications, accurate knowledge of this parameter is very important but at the same time very difficult to estimate. Based on the preceding, ERT applications are more suitable for small field application areas with small hydraulic gradients, a fact that concurs with the concept of this paper which investigates point-source contamination from OOWM that are usually found in small extents.

Conclusions

This paper has focused on the combination of geophysical imaging techniques and numerical modeling in order to investigate the transport of OOMW in a soil laboratory column under unsaturated-saturated conditions. Geophysical techniques provide an additional data source for groundwater model calibration, specifically in cases where sparse or no concentration data are available.

Electrical resistivity imaging data of the plume movement through the soil column were taken in specific time steps and were used as a surrogate for contaminant concentration measurements for the calibration of the numerical model. The finite element flow and transport model FEFLOW was employed for this purpose and was calibrated using the diffusion parameter.

A statistical analysis showed a very good agreement between the geophysical imaging data and the FEFLOW modeling results. The results indicated that in the unsaturated zone, the FEFLOW numerical model always reaches the designated layer slightly earlier than the geophysical images, while in the saturated zone the exact opposite occurs. This mismatch could be attributed to the water drainage at the bottom of the tank that might have affected the contaminant migration and so the ERT images. Regarding the sensitivity analysis results, the porosity seems to be the most sensitive parameter for the flow and transport model.

This controlled experiment demonstrates that geophysical methods can provide valuable information for the calibration of simulation models in small-scale field applications in cases where contaminant concentration measurements are scarce and boundary conditions are well known. Nevertheless, to increase the robustness of the aforementioned statement, it should be verified by additional laboratory experiments under different configurations, soil and contaminant types in order to investigate their effect on both the resistivity data and transport modeling.

Acknowledgements The project is co-funded by the European Social Fund and National Resources in the framework of the project THALIS (32-4-4), entitled "GEODIAMETRIS – Integrated Geoinformatics Technologies for Time-Lapse Monitoring of Land Pollution from the Disposal of Olive-Oil Mills Waste". Dr. Tobias Geyer is thanked for his valuable support in this work and comments made for improving the manuscript. We are grateful also to Dr. Hasan Aktarakçi from the AGI, who re-processed the resistivity data using the sand box module of the Earth Imaging 3D software. Our gratitude also goes to Prof. Allen Bateman, for his detailed explanation about the 'Brazil nut effect' and granular convection phenomenon. We wish to thank also Prof. E. Steiakakis and Prof. K. Komnitsas for estimating the hydraulic parameters of the soil and providing the chemical analysis of the OOMW, respectively.

References

- Al-Darby A, Abdel-Nasser G (2006) Nitrate leaching through unsaturated soil columns: comparison between numerical and analytical solutions. *J Appl Sci* 6(4):735–743
- ANSYS (2011) ANSYS Mechanical, ANSYS, Canonsburg, PA

- APHA (1999) Standard methods for the examination of water and wastewater, method 5530, 20th edn. American Public Health Association, Washington, DC
- Badv K, Faridfarid MR (2005) Laboratory determination of water retention and diffusion coefficient in unsaturated sand. *Water Air Soil Pollut* 161:25–38
- Bentley L, Gharibi M (2004) Two- and three-dimensional electrical resistivity imaging at a heterogeneous remediation site. *Geophysics* 69(3):674–680
- Bing Z, Greenhalgh S (2000) Cross-hole resistivity tomography using different electrode configurations. *Geophys Prospect* 48:887–912. doi:10.1046/j.1365-2478.2000.00220.x
- Binley A, Cassiani G, Middleton R, Winship P (2002a) Vadose zone flow model parameterisation using cross-borehole radar and resistivity imaging. *J Hydrol* 267:147–159
- Binley A, Winship P, West LJ, Pokar M, Middleton R (2002b) Seasonal variation of moisture content in unsaturated sandstone inferred from borehole radar and resistivity profiles. *J Hydrol* 267:160–172
- Bloem E, French HK, Binley A, Schotanus D, Eggen G (2010), Time-lapse resistivity measurements combined with soil water sampling to characterize solute movement in the unsaturated zone at Oslo airport, Gardermoen. Fall Meeting 2010, Abstract no. H13G-04, American Geophysical Union, Washington, DC
- Candansayar ME (2008) Two-dimensional individual and joint inversion of three- and four-electrode array DC resistivity data. *J Geophys Eng* 5:290–300
- Cassiani G, Binley A (2005) Modeling unsaturated flow in a layered formation under quasi-steady state conditions using geophysical data constraints. *Adv Water Resour* 28:467–477
- Cassiani G, Bruno V, Villa A, Fusi N, Binley AM (2006) A saline trace test monitored via time-lapse surface electrical resistivity tomography. *J Appl Geophys* 59(3):244–259
- Coscia I, Niklas L, Stewart G, Tobias V, Alan G (2012) Estimating traveltimes and groundwater flow patterns using 3D time-lapse crosshole ERT imaging of electrical resistivity fluctuations induced by infiltrating river water. *Geophysics* 77(4):E239–E250. doi:10.1190/geo2011-0328.1
- Culver TB, Hallisey SP, Sahoo D, Deitsch JJ, Smith JA (1997) Modeling the desorption of organic contaminants from long-term contaminated soil using distributed mass transfer rates. *Environ Sci Technol* 31(6):1581–1588
- Daily W, Ramirez A, LaBrecque D, Nitao J (1992) Electrical resistivity tomography of vadose water movement. *Water Resour Res* 28(5):1429–1442
- Diersch H-JG (2002) FEFLOW: physical basis of modeling. Reference manual, WASY, Berlin
- Diersch H-JG (2009) FEFLOW: finite element subsurface flow and transport simulation system. Reference manual. WASY, Berlin, 292 pp
- Doetsch J, Linde N, Vogt T, Binley A, Green AG (2012) Imaging and quantifying salt-tracer transport in a riparian groundwater system by means of 3D ERT monitoring. *Geophysics* 77(5):B207. doi:10.1190/geo2012-0046.1
- Dokou Z, Karatzas G (2012) Saltwater intrusion estimation in a karstified coastal system using density-dependent modelling and comparison with the Ghyben-Herzberg approach. *Hydrol Sci J* 57(5):985–999
- EarthImager 3D (2008) Resistivity inversion software manual, version 1.5.3. Advanced Geosciences, Austin, TX
- Fiore S, Zanetti MC (2009) Sorption of phenols: influence of groundwater pH and of soil organic carbon content. *Am J Environ Sci* 5(4):546–554
- Gasperikova E, Hubbard SS, Watson DB, Baker GS, Peterson JE, Kowalsky MB, Smith M, Brooks S (2012) Long-term electrical resistivity monitoring of recharge-induced contaminant plume behavior. *J Contam Hydrol* 142–143:33–49
- Grossman EL (1997) The effects of container geometry on granular convection. *Phys Rev E* 56:3290
- Herbert AW, Jackson CP, Lever DA (1988) Coupled groundwater flow and solute transport with fluid density strongly dependent upon concentration. *Water Resour Res* 24(10):1781–1794
- Irving J, Singha K (2010) Stochastic inversion of tracer test and electrical geophysical data to estimate hydraulic conductivities. *Water Resour Res* 46, W11514. doi:10.1029/2009WR008340

- Jakovovic D, Werner AD, Simmons CT (2011) Numerical modeling of saltwater up-coning: comparison with experimental laboratory observations. *J Hydrol* 402(3–4):261–273
- Jardani A, Revil A, Dupont JP (2012) Stochastic joint inversion of hydrogeophysical data for salt tracer test monitoring and hydraulic conductivity imaging. *Adv Water Resour* 52:62–77
- Johnson T, Versteeg R, Rockhold M, Slater L, Ntarlagiannis D, Greenwood W, Zachara J (2012) Characterization of a contaminated wellfield using 3D electrical resistivity tomography implemented with geostatistical, discontinuous boundary, and known conductivity constraints. *Geophysics* 77(6):EN85–EN96. doi:10.1190/geo2012-0121.1
- Karaoulis M, Revil A, Werkem D, Minsley B, Woodruff W, Kemna A (2011) Time-lapse three-dimensional inversion of complex conductivity data using an active time constrained (ATC) approach. *Geophys J Int* 187:237–251
- Kemna A, Vanderborght J, Kulessa B, Vereecken H (2002) Imaging and characterisation of subsurface solute transport using electrical resistivity tomography (ERT) and equivalent transport models. *J Hydrol* 267:125–146
- Kim J-H, Yi MJ, Park SG, Kim JG (2009) 4-D inversion of DC resistivity monitoring data acquired over a dynamically changing earth model. *J Appl Geophys* 68(4):522–532
- Knight JB, Jaeger HM, Nagel S (1993) Vibration-induced size separation in granular media: the convection connection. *Phys Rev Lett* 70:3728
- Knight JB, Ehrichs EE, Kuperman VY, Flint JK, Jaeger HM, Nagel SR (1996) Experimental study of granular convection. *Phys Rev E* 54:5726
- Koukadaki MA, Karatzas GP, Papadopoulou MP, Vafidis A (2007) Identification of the saline zone in a coastal aquifer using electrical tomography data and simulation. *Water Resour Manag* 21:1881–1898. doi:10.1007/s11269-006-9135-y
- LaBrecque DJ, Morelli G, Daily WA, Ramirez A, Lundegard P (1997), Occam's inversion of 3-D electrical resistivity tomography. In: Oristaglio M, Spies B (eds) Three-dimensional electromagnetics. Society of Exploration Geophysicists, Tulsa, OK, pp 575–590
- Leontarakis K, Apostolopoulos GV (2012) Laboratory study of the cross-hole resistivity tomography: the model stacking (MOST) technique. *J Appl Geophys* 80:67–82
- Lin HJ, Richards DR, Talbot CA, Yeh G-T, Cheng J, Cheng H (1997) FEMWATER: a three-dimensional finite element computer model for simulating density-dependent flow and transport in variably saturated media. Technical Report CHL-97-12, US Army Corps of Engineers, Washington, DC and Pennsylvania State University, University Park, PA
- Loke MH, Barker RD (1996) Rapid least squares inversion of apparent resistivity pseudosections by a quasi-Newton method. *Geophys Prospect* 44:131–152
- Lydakis-Simantiris N, Anastopoulos M, Terzis E, Vozinakis K (2005) Determination of phenols in river waters: a case study for Keritis River at northwestern Crete. Proceedings of the 2005 WSEAS International Conference on Engineering Education, Athens, Greece, July 2005, pp 446–451
- Majken CL, Karsten H, Jensen AB, Nielsen L (2008) Monitoring unsaturated flow and transport using cross-borehole geophysical methods. *Vadose Zone J* 7(1):227–237. doi:10.2136/vzj2006.0129
- Mantzavinos D, Kalogerakis N (2005) Treatment of olive mill effluents, part 1: organic matter degradation by chemical and biological processes: an overview. *Environ Int* 31(2):289–295
- Mirbagheri SA (2004) Modeling contaminant transport in soil column and ground water pollution control. *Int J Environ Sci Technol* 1(2):141–150
- Mirbagheri SA, Monfared HSA (2009) Pesticide transport and transformation modeling in soil column and groundwater contamination prediction. *Int J Environ Sci Technol* 6(2):233–242
- Moraetis D, Stamati FE, Nikolaidis NP, Kalogerakis N (2011) Olive mill wastewater irrigation of maize: impacts on soil and groundwater. *Agric Water Manage* 98:1125–1132
- Müller KJ, Vanderborght A, Englert A, Kemna J, Huisman A, Rings J, Vereecken H (2010) Imaging and characterization of solute transport during two tracer tests in a shallow aquifer using electrical resistivity tomography and multilevel groundwater samplers. *Water Resour Res* 46, W03502. doi:10.1029/2008WR007595
- Osiensky JL, Donaldson PR (1995) Electrical flow through an aquifer for contaminant source leak detection and delineation of plume evolution. *J Hydrol* 169:243–263
- Pankow JF, Rathbun RE, Zogorski JS (1996) Calculated volatilization rates of fuel oxygenate compounds and other gasoline-related compounds from river and streams. *Chemosphere* 33:921–937
- Peleg N, Gvirtzman H (2010) Groundwater flow modeling of two-levels perched karstic leaking aquifers as a tool for estimating recharge and hydraulic parameters. *J Hydrol* 388:13–27
- Perri MT, Cassiani G, Gervasio I, Deiana R, Binley A (2012) A saline tracer test monitored via both surface and cross-borehole electrical resistivity tomography: comparison of time-lapse results. *J Appl Geophys* 79:6–16
- Piotrowska A, Lamarino G, Antonietta RM, Gianfreda L (2006) Short-term effects of olive mill waste water (OMW) on chemical and biochemical properties of a semiarid Mediterranean soil. *Soil Biol Biochem* 38:600–610
- Rivett MO, Clark L (2007) A quest to locate sites described in the world's first publication on trichloroethene contamination of groundwater. *J Eng Geol Hydrogeol* 40(3):241–249. doi:10.1144/1470-9236/06-047
- Rong Y (1999) A study of vadose zone transport model VLEACH. *J Soil Contam* 8(2):217–229
- Rubin Y, Hubbard S (eds) (2005) Hydrogeophysics, series: Water Science and Technology Library, vol 50. Springer, Heidelberg, Germany
- Sasaki Y (1992) Resolution of resistivity tomography inferred from numerical simulation. *Geophys Prospect* 40:453–63
- Seferou P (2011) Characterization of unsaturated flow and transport in porous deposits with hydrogeophysical laboratory methods. MSc Thesis, Georg-August Universität – Göttingen, Hydrogeology and Environment Geosciences (HEG), Germany
- Sasaki Y (1994) 3-D resistivity inversion using the finite-element method. *Geophysics* 59:1839–1848
- Slater L, Zaidman MD, Binley AM, West LJ (1997) Electrical imaging of saline tracer migration for the investigation of unsaturated zone transport mechanisms. *Hydrol Earth Syst Sci* 1(2):291–302
- Slater L, Versteeg R, Binley A, Cassiani G, Birken R, Sandberg S (2002) A 3D ERT study of solute transport in a large experimental tank. *J Appl Geophys* 49:211–229
- Smith CJ, Perfetti TA, Morton MJ, Rodgman A, Garg R, Selassie CD, Hansch C (2002) The relative toxicity of substituted phenols reported in cigarette mainstream smoke. *Toxicol Sci* 69:265–278
- Swanson RD, Singha K, Day-Lewis FD, Binley A, Keating K, Haggerty R (2012) Direct geoelectrical evidence of mass transfer at the laboratory scale. *Water Resour Res* 48, W10543. doi:10.1029/2012WR012431
- Tait NG, Davison RM, Whittaker JJ, Leharne SA, Lerner DN (2004) Borehole optimisation system (BOS): a GIS-based risk analysis tool for optimising the use of urban ground water. *Environ Model Softw* 19:1111–1124
- Tsagaraki E, Lazarides HN, Petrotos KB (2007) Olive mill wastewater treatment. In: Oreopoulou V, Winfried R (eds) Utilization of by-products and treatment of waste in the food industry. Springer, New York, pp 133–157
- van Genuchten M-Th (1978) Mass transport in saturated-unsaturated media: one-dimensional solutions. Research Rep. no. 87-WR-11, Water Resources Program, Princeton University, Princeton, NJ
- Ward AS, Gooseff MN, Singha K (2010) Characterizing hyporheic transport processes: interpretation of electrical geophysical data in coupled stream-hyporheic zone systems during solute tracer studies. *Adv Water Resour* 33(11):1320–1330
- Zenjari B, Neimeddine A (2001) Impact of spreading olive mill wastewater on soil characteristics: laboratory experiments. *Agronomie* 21:749–755